On the influence of the hysteretic behavior of the capillary pressure on the wave propagation in partially saturated soils

Bettina Albers

Einstein Junior Fellow, TU Berlin, Soil Mechanics and Geotechnical Engineering, Sekr. TIB1-B7, Gustav-Meyer-Allee 25, 13355 Berlin, Germany

E-mail: albers@grundbau.tu-berlin.de

Abstract. It is well known that the capillary pressure curve of partially saturated soils exhibits a hysteresis. For the same degree of saturation it has different values depending on the initial state of the soil, thus for drying of a wet soil or wetting of a dry soil. The influence of these different values of the capillary pressure on the propagation of sound waves is studied by use of a linear hyperbolic model. Even if the model does not contain a hysteresis operator, the effect of hysteresis in the capillary pressure curve is accounted for. In order to obtain the limits of phase speeds and attenuations for the two processes the correspondent values for main drying and main wetting are inserted into the model separately. This is done for two examples of soils, namely for Del Monte sand and for a silt loam both filled by an air-water mixture. The wave analysis reveals four waves: one transversal wave and three longitudinal waves. The waves which are driven by the immiscible pore fluids are influenced by the hysteresis in the capillary pressure curve while the waves which are mainly driven by the solid are not.

1. Introduction

The capillary pressure or suction curve of partially saturated soils (i.e. of soils whose pore space is filled by a mixture of immiscible fluids) exhibits different values for the same degree of saturation depending on whether water is drained or supplied. This phenomenon, known as soil-moisture hysteresis, is discussed in details in [1]. Measuring methods, the prediction of capillary pressure curves from measured data and first results on the influence of drying and wetting on the propagation of sound waves are addressed in [2].

In the present paper the examination of the influence of the hysteresis on the wave propagation is deepened by comparing the behavior of two soil types whose capillary pressure curves along with experimentally observed values have been presented in [3]. The experimental and predicted values of Del Monte sand and "EFEDA" silt loam are illustrated in [3].

For the sand the main drying curve (MDC) has been measured. The main wetting curve (MWC) has been predicted using the measured data. Measurements of the capillary pressure curves are time consuming and often one measurement technique is not sufficient to cover the large range of capillary pressures which mostly spans certain orders of magnitude. For the silt loam even both main curves have been predicted from measurements of the primary wetting curve (PWC) and scanning drying curves (SDC). The latter are inner hysteresis curves which appear upon redrying and rewetting. The prediction method, proposed by Haverkamp et al. [3]

implies that all drying and wetting curves, regardless of the scanning order, have the shape of the van Genuchten equation [4] in normalized form

$$\theta^* = \frac{\theta - \theta_r}{\theta_S - \theta_r} = \left[1 + \left(\frac{h}{h_g}\right)^n\right]^{-m}, \tag{1}$$

where θ is the volumetric water content, θ_r the residual water content, θ_s the water content at natural saturation, h the soil water pressure head or matric potential, h_g a van Genuchten pressure head scale parameter and n and m are van Genuchten shape parameters.

This leads to the following equations for the MWC and the MDC

$$\theta^*_{mw} \equiv \frac{\theta_{mw}}{\theta_{Smw}} = \left[1 + \left(\frac{h}{h_{gmw}}\right)^{n_{mw}}\right]^{-m_{mw}}, \quad \theta^*_{md} \equiv \frac{\theta_{md}}{\theta_{Smd}} = \left[1 + \left(\frac{h}{h_{gmd}}\right)^{n_{md}}\right]^{-m_{md}}, \tag{2}$$

where the subscripts mw and md refer to main wetting and main drying, respectively. The relations between the specific wetting parameters m_{mw}, n_{mw} and h_{gmw} and the drying parameters m_{md}, n_{md} and h_{gmd} are specified in [3] in the following way

$$\begin{matrix} m_{mw} = m_{md}, \\ n_{mw} = n_{md}, \end{matrix} \qquad \text{and} \qquad h_{gmd} = 2h_{gmw}, \quad \text{for} \quad \begin{cases} m_{mw}n_{mw} \geq 1, \\ m_{md}n_{md} \geq 1. \end{cases} \tag{3}$$

The prediction of several curves of different scanning order from measured data has been demonstrated in [3] for 22 different soil samples. Two of them (sand and silt loam) are used here to calculate the wave speeds and attenuations of the waves occurring if the pore space of the soil contains the immiscible pore fluids water and air. The possible range of the acoustic properties is determined by calculating them for the limit cases. This means, that separately the values of the MDC and of the MWC are used in the relation between capillary pressure and saturation.

The material properties of the two soil types are summarized in Table 1. Some of them are given in [3]. Others have been calculated using e.g. the value of the earth acceleration $g = 9.81$ m s^{-2} and the conversion of the pressure head in cm H_2O (used in [3]) into the capillary pressure in Pa (used in the continuum model)

$$\text{pressure head } h \text{ [m H}_2\text{O]} = \frac{\text{capillary pressure } p_c \text{ [Pa]}}{\rho^{FR} \text{ [kg m}^{-3}\text{] } g \text{ [m s}^{-2}\text{]}} \quad \Rightarrow \quad 1\text{[cm H}_2\text{O]} = 100\text{[Pa]}.$$

The dimensional van Genuchten scale parameters α for drying and wetting, used in the continuum model, have been calculated from the head scale parameters given in [3] by

$$\alpha_{d/w} \text{ [Pa]} = \frac{1}{10 \; g \text{ [m s}^{-2}\text{] } h_{gd/gw} \text{ [cm]}.}$$

The material parameters connected with the properties of the solid, as e.g. porosity, mass density and Poisson's ratio, have been ascertained in the literature.

The example of Del Monte sand is widely studied and the material parameters for this soil type, given in [5], have been used even if they deviate from experienced data for sandy soils classified in the German standard DIN 4220 (compare [6]). For the porosity of Del Monte sand the authors of [5] refer to measurements of Liakopoulos who measured also the MDC data [7]. The reported value of the initial porosity $n_0 = 0.2975$ is used also here even if in the literature more plausible bigger values between 34.5% and 37% are mentioned. Also the Poisson ratio of 0.4 seems rather high and the solid grain density of 2000 kg m^{-3} rather low.

Table 1. Material properties of Del Monte sand and loam silt filled by an air-water mixture.

	Del Monte sand	silt loam
real compressibility grains K_s [GPa]	35	35
real compressibility fluid K_f [GPa]	2.25	2.25
real compressibility gas K_g [MPa]	0.101	0.101
Poisson's ratio ν [-]	0.4	0.35
shear modulus μ^S [GPa]	0.4724	0.4487
solid grain density ρ^{SR} [kg m^{-3}]	2000	2650
fluid density ρ^{FR} [kg m^{-3}]	1000	1000
initial porosity n_0 [-]	0.2975	0.5
intrinsic permeability k [m^2]	$4.5 \cdot 10^{-13}$	$1.92 \cdot 10^{-13}$
water conductivity $\mathrm{K} = k\frac{\rho^{FR}g}{\mu_w}$ [m/s]	$4.44 \cdot 10^{-6}$	$1.888 \cdot 10^{-6}$
water resistance $\pi^F = \frac{n_0\rho^{FR}g}{\mathrm{K}}$ [kg m^{-3}s^{-1}]	$6.573 \cdot 10^8$	$2.598 \cdot 10^9$
air resistance π^G [kg m^{-3}s^{-1}]	$1.82 \cdot 10^5$	$1.82 \cdot 10^5$
water viscosity μ_w [Pa s]	$1 \cdot 10^{-3}$	$1 \cdot 10^{-3}$
air viscosity μ_a [Pa s]	$1.82 \cdot 10^{-5}$	$1.82 \cdot 10^{-5}$
van Genuchten parameter n [-]	4.150	4.556
van Genuchten parameter m [-]	0.518	0.561
h_g for drying [cm]	116.56	720.520
h_g for wetting [cm]	58.28	360.26
α for drying [Pa]	0.000087454	0.000014147
α for wetting [Pa]	0.000174909	0.000028295

The material parameters of the silt loam (see Table 1) are in better accordance to the values given for similar soil types classified in DIN 4220.

Two different approaches for the estimation of the shear modulus have been compared in [8]. Here, the expression stemming from classical elasticity is used

$$\mu^S = \frac{3}{2}\frac{1-2\nu}{1+\nu}\frac{K_s}{1+50n_0}. \tag{4}$$

The last term is the widely used Geertsma formula for the drained compressibility modulus $K_d = K_s/(1+50n_0)$ (see e.g. [9]).

Also at high values of capillary pressure a certain quantity of water (the amount depends on the soil type) remains in the sample. For both soil types this so-called irreducible saturation is very small. Therefore, nearly the whole range of initial saturations $0.01 \leq S_0 \leq 1$ is studied in this paper.

2. Linear model for partially saturated soils

The book [6] deals with the modeling of partially saturated soils and the analysis of sound wave propagation in one-, two- and three-component media. A hyperbolic linear model which is able to describe the wave propagation is introduced and analyzed. However, this model only accounts for one branch of the capillary pressure curve. The saturation-capillary pressure-relation enters the model in form of the van Genuchten equation [4] as a constitutive law. Since this relation and also the measurable material parameters are microscopic but the model is macroscopic, all quantities have to be transferred from the micro- to the macro-scale. The macroscopic material parameters $\left\{\lambda^S + \frac{2}{3}\mu^S, \kappa^F, \kappa^G, Q^F, Q^G, Q^{FG}\right\}$ follow from the initial porosity n_0, the real compressibilities of solid, fluid and gas, K_s, K_f and K_g, respectively, together with the above quoted Geertsma formula and the van Genuchten law (1) in the notation of the continuum model

$$p_c = \frac{1}{\alpha}\left[S^{(-1/m)} - 1\right]^{1/n}, \tag{5}$$

where S denotes the degree of saturation, p_c the capillary pressure and α, n and m the van Genuchten parameters. λ^S and μ^S are Lamé parameters, κ^F and κ^G are the compressibilities of fluid and gas. Q^F, Q^G and Q^{FG} are coupling parameters between solid-fluid, solid-gas and fluid-gas, respectively. They appear in the macroscopic set of field equations

$$\begin{aligned}
\rho_0^S \frac{\partial \mathbf{v}^S}{\partial t} &= \operatorname{div}\left\{\lambda^S e\mathbf{1} + 2\mu^S \mathbf{e}^S + Q^F \varepsilon^F \mathbf{1} + Q^G \varepsilon^G \mathbf{1}\right\} + \\
&\quad + \pi^{FS}\left(\mathbf{v}^F - \mathbf{v}^S\right) + \pi^{GS}\left(\mathbf{v}^G - \mathbf{v}^S\right), \\
\rho_0^F \frac{\partial \mathbf{v}^F}{\partial t} &= \operatorname{grad}\left\{\rho_0^F \kappa^F \varepsilon^F + Q^F e + Q^{FG}\varepsilon^G\right\} - \pi^{FS}\left(\mathbf{v}^F - \mathbf{v}^S\right), \\
\rho_0^G \frac{\partial \mathbf{v}^G}{\partial t} &= \operatorname{grad}\left\{\rho_0^G \kappa^G \varepsilon^G + Q^G e + Q^{FG}\varepsilon^F\right\} - \pi^{GS}\left(\mathbf{v}^G - \mathbf{v}^S\right), \\
\frac{\partial \mathbf{e}^S}{\partial t} &= \operatorname{sym}\operatorname{grad}\mathbf{v}^S, \quad \frac{\partial \varepsilon^F}{\partial t} = \operatorname{div}\mathbf{v}^F, \quad \frac{\partial \varepsilon^G}{\partial t} = \operatorname{div}\mathbf{v}^G, \quad e \equiv \operatorname{tr}\mathbf{e}^S.
\end{aligned} \tag{6}$$

The fields $\left\{\mathbf{v}^S, \mathbf{v}^F, \mathbf{v}^G, \mathbf{e}^S, \varepsilon^F, \varepsilon^G\right\}$ are the velocities of the three components, the macroscopic deformation tensor $\mathbf{e}^S$ and the volume changes of fluid and gas, respectively.

The volume changes of the solid, fluid and gas, $e, \varepsilon^F, \varepsilon^G$, are defined by

$$e = \frac{\rho_0^S - \rho^S}{\rho_0^S}, \quad \varepsilon^F = \frac{\rho_0^F - \rho^F}{\rho_0^F}, \quad \varepsilon^G = \frac{\rho_0^G - \rho^G}{\rho_0^G}, \tag{7}$$

where ρ^S, ρ^F and ρ^G are the partial mass densities of the components. Quantities with subindex zero are initial values of the corresponding current quantities.

Moreover, in (6) the relative resistances π^{FS} and π^{GS} of the flow of the pore fluids through the channels of the skeleton occur. Taking into account formulae for the relative permeabilities k_f and k_g proposed by van Genuchten [4]

$$k_f = S^{\frac{1}{2}}\left[1 - \left(1 - S^{\frac{1}{m}}\right)^m\right]^2, \qquad k_g = (1-S)^{\frac{1}{3}}\left(1 - S^{\frac{1}{m}}\right)^{2m}. \tag{8}$$

and the parameters π^F and π^G incorporating the permeability of the solid and the viscosity of the pore fluid (see Table 1) the resistances are calculated by

$$\pi^{FS} = \frac{\pi^F}{k_f}, \qquad \pi^{GS} = \frac{\pi^G}{k_g}. \tag{9}$$

3. Propagation of sound waves

By means of the set (6) the propagation of sound waves in partially saturated sand and silt loam is studied. In order to describe the propagation of plane monochromatic waves in an infinite medium whose fronts are perpendicular to the unit vector in the direction of propagation $\mathbf{n}$, we suppose

$$\begin{gathered}
\varepsilon^F = E^F \mathcal{E}, \quad \varepsilon^G = E^G \mathcal{E}, \quad \mathbf{e}^S = \mathbf{E}^S \mathcal{E}, \\
\mathbf{v}^F = \mathbf{V}^F \mathcal{E}, \quad \mathbf{v}^G = \mathbf{V}^G \mathcal{E}, \quad \mathbf{v}^S = \mathbf{V}^S \mathcal{E}, \\
\mathcal{E} := \exp i\left(\mathbf{k}\cdot\mathbf{x} - \omega t\right),
\end{gathered} \tag{10}$$

where $\mathbf{E}^S, E^F, E^G, \mathbf{V}^S, \mathbf{V}^F, \mathbf{V}^G$ are constant amplitudes, ω is a given frequency and $\mathbf{k} = k\mathbf{n}$ is the wave vector with the complex wave number k.

The compatibility relations

$$
\begin{aligned}
&E^F = -\frac{1}{\omega} k\mathbf{n} \cdot \mathbf{V}^F, \quad E^G = -\frac{1}{\omega} k\mathbf{n} \cdot \mathbf{V}^G, \\
&\mathbf{E}^S = -\frac{1}{2\omega} k \left(\mathbf{n} \otimes \mathbf{V}^S + \mathbf{V}^S \otimes \mathbf{n} \right), \quad \text{i.e.} \quad e = -\frac{1}{\omega} k\mathbf{n} \cdot \mathbf{V}^S \mathcal{E},
\end{aligned} \tag{11}
$$

follow from substitution of (10) into the last line of (6). Using (11) in the remaining field equations leads to

$$
\begin{aligned}
\omega^2 \mathbf{V}^S = &\frac{\lambda^S}{\rho_0^S} k^2 \left(\mathbf{V}^S \cdot \mathbf{n} \right) \mathbf{n} + \frac{\mu^S}{\rho_0^S} k^2 \left(\left(\mathbf{V}^S \cdot \mathbf{n} \right) \mathbf{n} + \mathbf{V}^S \right) + \\
&+ \frac{Q^F}{\rho_0^S} k^2 \left(\mathbf{V}^F \cdot \mathbf{n} \right) \mathbf{n} + \frac{Q^G}{\rho_0^S} k^2 \left(\mathbf{V}^G \cdot \mathbf{n} \right) \mathbf{n} + \\
&+ i \frac{\pi^{FS} \omega}{\rho_0^S} \left(\mathbf{V}^F - \mathbf{V}^S \right) + i \frac{\pi^{GS} \omega}{\rho_0^S} \left(\mathbf{V}^G - \mathbf{V}^S \right) = 0,
\end{aligned} \tag{12}
$$

$$
\begin{aligned}
&\omega^2 \mathbf{V}^F = \kappa^F k^2 \left(\mathbf{V}^F \cdot \mathbf{n} \right) \mathbf{n} + \frac{Q^F}{\rho_0^F} k^2 \left(\mathbf{V}^S \cdot \mathbf{n} \right) \mathbf{n} + \\
&+ \frac{Q^{FG}}{\rho_0^F} k^2 \left(\mathbf{V}^G \cdot \mathbf{n} \right) \mathbf{n} - i \frac{\pi^{FS} \omega}{\rho_0^F} \left(\mathbf{V}^F - \mathbf{V}^S \right) = 0,
\end{aligned} \tag{13}
$$

$$
\begin{aligned}
&\omega^2 \mathbf{V}^G = \kappa^G k^2 \left(\mathbf{V}^G \cdot \mathbf{n} \right) \mathbf{n} + \frac{Q^G}{\rho_0^G} k^2 \left(\mathbf{V}^S \cdot \mathbf{n} \right) \mathbf{n} + \\
&+ \frac{Q^{FG}}{\rho_0^G} k^2 \left(\mathbf{V}^F \cdot \mathbf{n} \right) \mathbf{n} - i \frac{\pi^{GS} \omega}{\rho_0^G} \left(\mathbf{V}^G - \mathbf{V}^S \right) = 0.
\end{aligned} \tag{14}
$$

The transversal wave follows, if the scalar product of (12)-(14) with an arbitrary unit vector $\mathbf{n}_\perp$ perpendicular to $\mathbf{n}$, i.e. $\mathbf{n} \cdot \mathbf{n}_\perp = 0$, is taken. This yields

$$
\begin{aligned}
&\omega^2 V_\perp^S = \frac{\mu^S}{\rho_0^S} k^2 V_\perp^S + i \frac{\pi^{FS} \omega}{\rho_0^S} \left(V_\perp^F - V_\perp^S \right) + i \frac{\pi^{GS} \omega}{\rho_0^S} \left(V_\perp^G - V_\perp^S \right), \\
&\omega^2 V_\perp^F = -i \frac{\pi^{FS} \omega}{\rho_0^F} \left(V_\perp^F - V_\perp^S \right), \qquad \omega^2 V_\perp^G = -i \frac{\pi^{GS} \omega}{\rho_0^G} \left(V_\perp^G - V_\perp^S \right), \\
&V_\perp^S := \mathbf{V}^S \cdot \mathbf{n}_\perp, \quad V_\perp^F := \mathbf{V}^F \cdot \mathbf{n}_\perp, \quad V_\perp^G := \mathbf{V}^G \cdot \mathbf{n}_\perp,
\end{aligned} \tag{15}
$$

and finally the dispersion relation for the shear wave.

In order to obtain relations for longitudinal waves the scalar product of equations (12)-(14) with the vector $\mathbf{n}$ is taken:

$$
\begin{aligned}
&\left\{ \omega^2 - \frac{\lambda^S + 2\mu^S}{\rho_0^S} k^2 + i \frac{\left(\pi^{FS} + \pi^{GS} \right) \omega}{\rho_0^S} \right\} V_\parallel^S - \\
&- \left\{ \frac{Q^F}{\rho_0^S} k^2 + i \frac{\pi^{FS} \omega}{\rho_0^S} \right\} V_\parallel^F - \left\{ \frac{Q^G}{\rho_0^S} k^2 + i \frac{\pi^{GS} \omega}{\rho_0^S} \right\} V_\parallel^G = 0, \\
&- \left\{ \frac{Q^F}{\rho_0^F} k^2 + i \frac{\pi^{FS} \omega}{\rho_0^F} \right\} V_\parallel^S + \left\{ \omega^2 - \kappa^F k^2 + i \frac{\pi^{FS} \omega}{\rho_0^F} \right\} V_\parallel^F - \frac{Q^{FG}}{\rho_0^F} k^2 V_\parallel^G = 0, \\
&- \left\{ \frac{Q^G}{\rho_0^G} k^2 + i \frac{\pi^{GS} \omega}{\rho_0^G} \right\} V_\parallel^S - \frac{Q^{FG}}{\rho_0^G} k^2 V_\parallel^F + \left\{ \omega^2 - \kappa^G k^2 + i \frac{\pi^{GS} \omega}{\rho_0^G} \right\} V_\parallel^G = 0,
\end{aligned} \tag{16}
$$

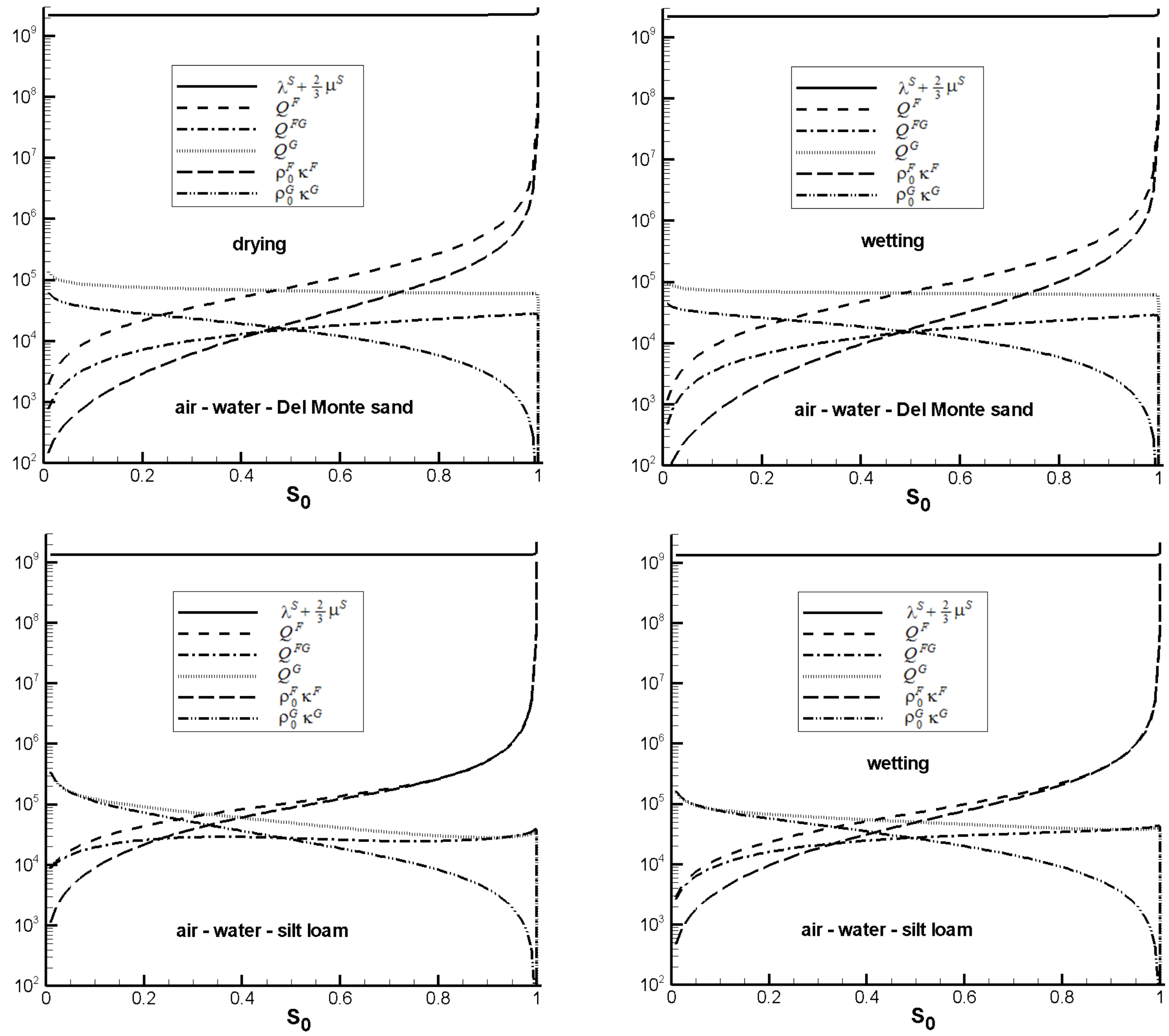

Figure 1. Macroscopic material parameters appearing in (6) in dependence on the initial saturation. Top row: Del Monte sand, bottom row: silt loam; for the parameters on the left hand side the MDC data, for those on the right hand side the MWC data have been used, respectively.

where

$$V_{\|}^S = \mathbf{V}^S \cdot \mathbf{n}, \quad V_{\|}^F = \mathbf{V}^F \cdot \mathbf{n}, \quad V_{\|}^G = \mathbf{V}^G \cdot \mathbf{n}. \tag{17}$$

The dispersion relations which, due to their lengthy form are not shown here, are solved for the complex wave number k. The results specify both the phase velocities $c_{ph} = \omega/\mathrm{Re}(k)$ and the attenuations $\mathrm{Im}(k)$.

4. Numerical results

The behavior of the waves propagating in Del Monte sand filled by an air-water mixture has been studied already in [10]. These results are compared here to those of a silt loam. As mentioned above, both soil types belong to those for which the capillary pressure curves are presented in [3].

4.1. Material parameters

The macroscopic material parameters of the model introduced in Section 2 have been calculated for both soil types from the microscopic material parameters summarized in Table 1. Once MDC data and once MWC data are used. The results are illustrated in Figure 1.

While for the sand a difference between the drying and the wetting data is hardly discernible, for the silt loam slight differences are visible. This does not only concern the numerical values but also the shape and, thus, the points of intersection of the curves.

We are interested in the influence of the consideration of different drying and wetting capillary pressure data on the propagation of sound waves. The behavior of the phase speeds and of the attenuations of the four appearing waves is examined in dependence on the frequency and on the initial saturation.

4.2. Frequency dependence

Figures 2 and 3 show for a single value of the initial saturation ($S_0 = 0.8$) the dependence of the phase speeds $\omega/\mathrm{Re}(k)$ and the attenuations $\mathrm{Im}(k)$ on the frequency. It is obvious that for

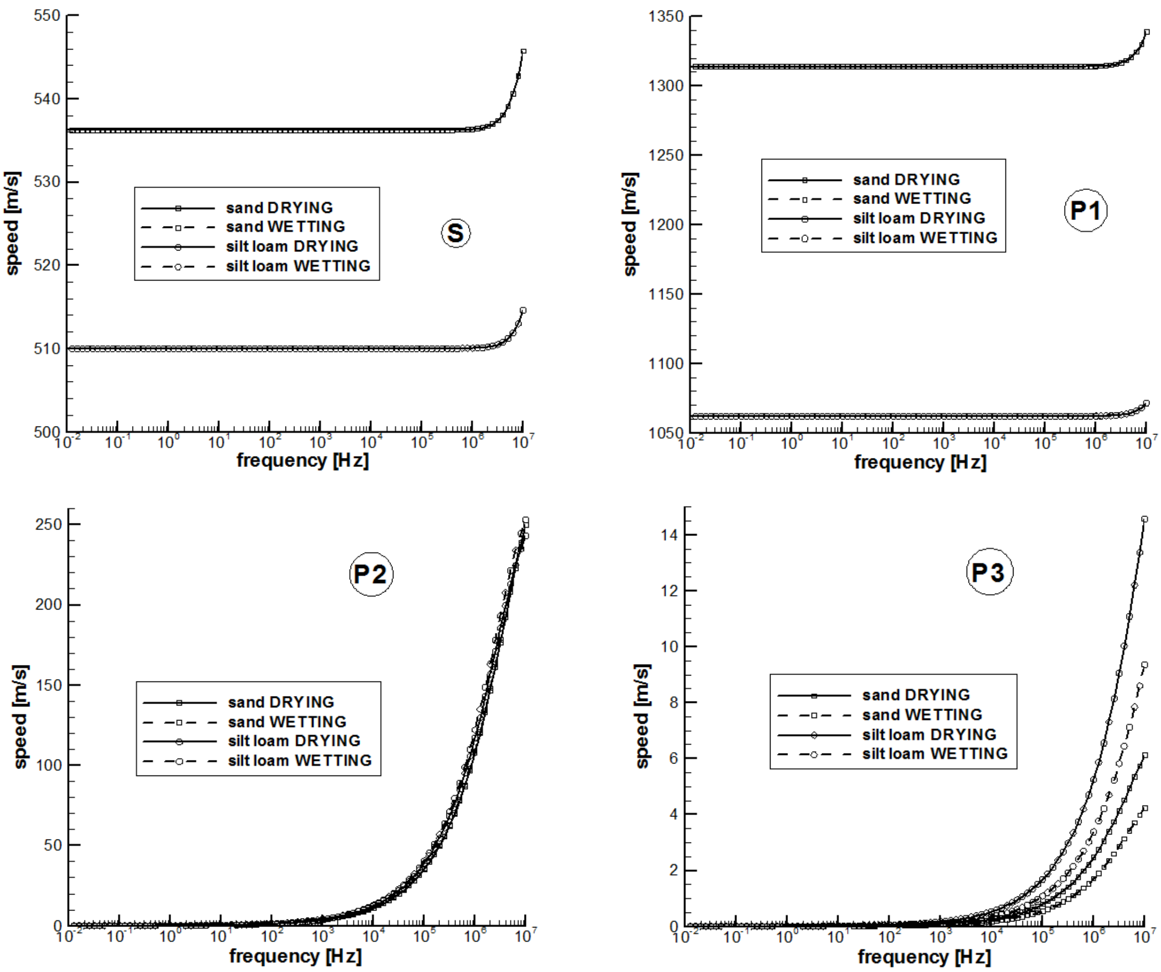

Figure 2. Phase speeds of the transversal wave S and the three longitudinal waves $P1$, $P2$ and $P3$ in dependence on the frequency ω using the parameters of the MDC (solid lines) and MWC (dashed lines) for Del Monte sand (squares) and silt loam (circles); $S_0 = 0.8$.

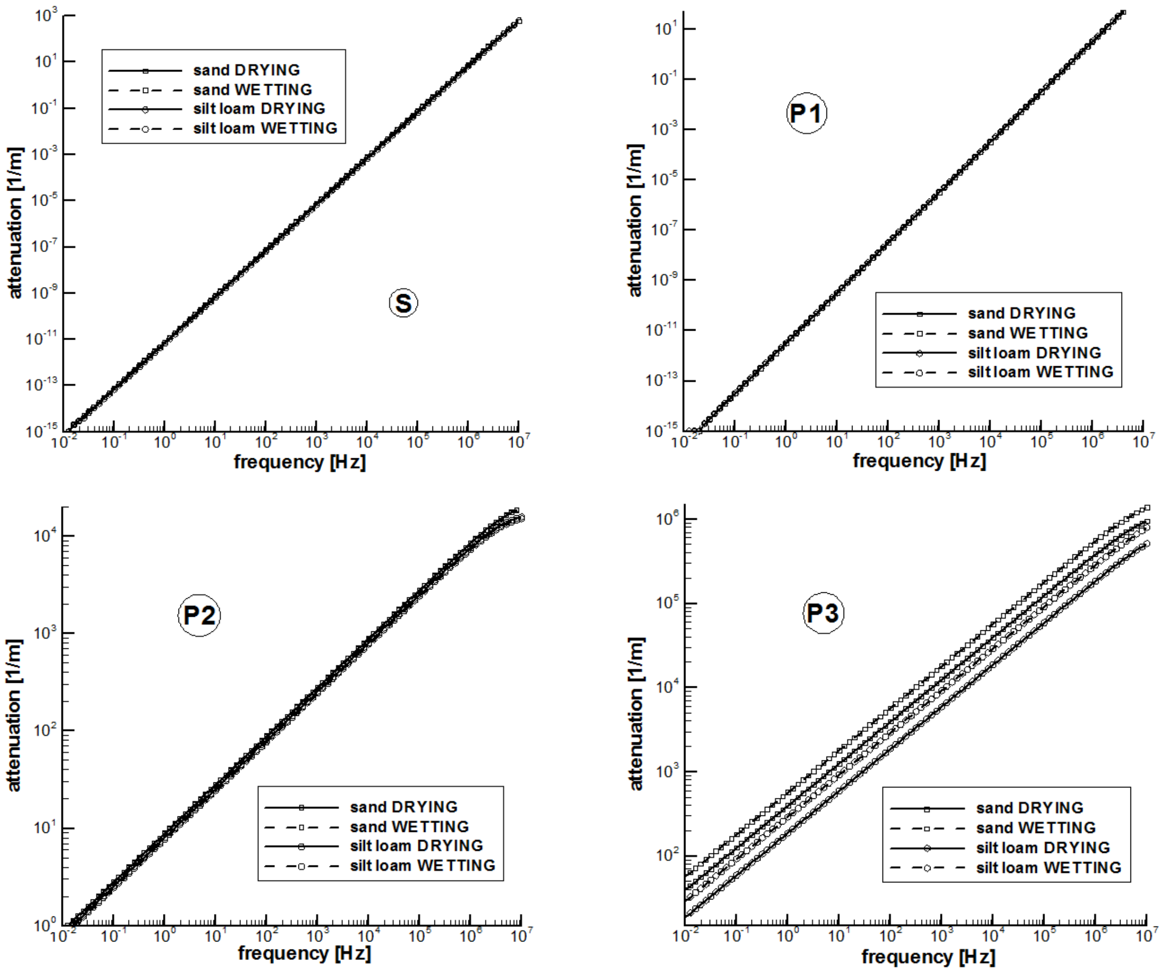

Figure 3. Attenuations of the transversal wave S and the three longitudinal waves $P1$, $P2$ and $P3$ in dependence on the frequency ω using the parameters of the MDC (solid lines) and MWC (dashed lines) for Del Monte sand (squares) and silt loam (circles); $S_0 = 0.8$.

the waves which are mainly influenced by the solid (the shear wave and the fast longitudinal wave $P1$) there is no difference at all between wetting and drying curves. Also for the waves which are driven by the pore fluids a difference occurs only for frequencies which do not appear in geophysical applications. In the next subsection we will have a closer look on what happens in dependence on the saturation for a smaller value of the frequency. The $P2$-wave appears also in saturated porous media and its speed depends on the compressibility of the pore fluid. It is slower than the first longitudinal wave. The third longitudinal wave appears due to capillary effects, i.e. it only appears if at least two immiscible pore fluids are present. Its speed is, again, much smaller than this of the $P2$-wave. Comparing the two soil types it can be observed that the speeds of the S- and $P1$-waves are higher for sand (due to the higher shear modulus and the smaller true solid mass density) while the speeds of the remaining two waves are higher in silt loam. However, the differences are small.

The same behavior becomes obvious inspecting the frequency dependence of the attenuations illustrated in Figure 3. Attenuations for drying and wetting data are the same for S and $P1$, barely distinguishable for $P2$ and different for $P3$. Presumably, the reason for the differences of the latter wave becoming evident is that the attenuation of this wave is extremely high. While

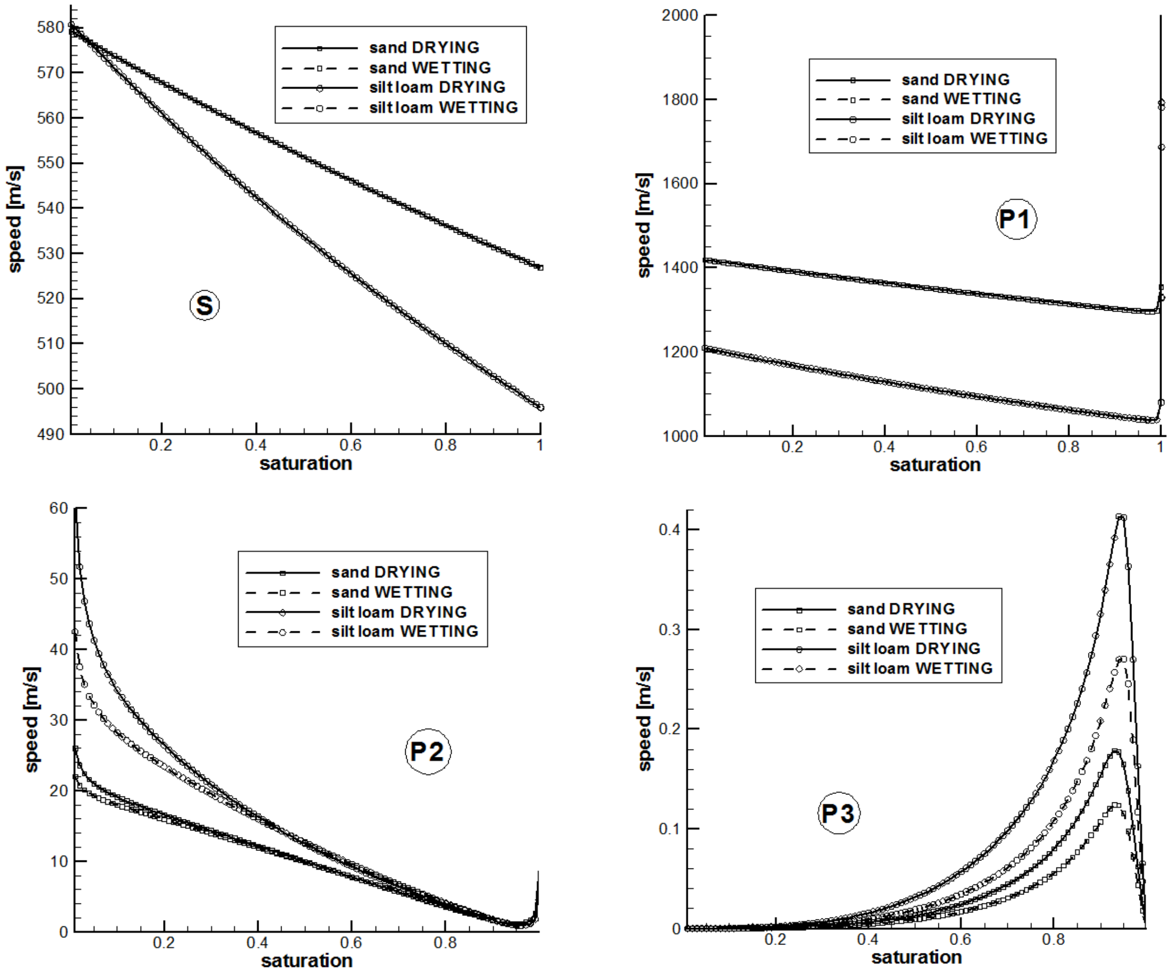

Figure 4. Phase speeds of the transversal wave S and the three longitudinal waves $P1$, $P2$ and $P3$ in dependence on the initial saturation S_0 using the parameters of the MDC (solid lines) and MWC (dashed lines) for Del Monte sand (squares) and silt loam (circles); $\omega = 1000$ Hz.

in the region of frequencies appearing in geophysical applications the attenuations of S- and $P1$-wave are of the order of 10^{-15} to 10^{-5} 1/m, for the $P3$-waves values of 10^1 to 10^4 1/m are observable. Such high values are barely measurable in practice. Already for the $P2$-wave whose attenuations for such frequencies are in the range of 1 to 100 1/m measurements were sophisticated but finally succeeded [11]. Attempts to measure speeds (very low) or attenuations (very high) of the $P3$-wave are not known. The theoretical values of the attenuation are bigger for drying than for wetting and higher for silt loam than for sand.

4.3. Dependence on the initial saturation

More interesting than the frequency dependence is the dependence of wave speeds and attenuations on the initial degree of saturation. To analyze this behavior we choose a frequency of 1000 Hz which is typical for geophysical applications.

The shear wave speed shows an almost linear behavior. It decreases for increasing degree of saturation. For a small initial saturation the speed for drying and wetting nearly coincides. It has a value of around 580 m/s. The decrease for bigger values of saturation is steeper for silt loam than it is for sand. While for silt loam it is approximately 14%, for sand around 9% are observable.

The speed of the $P1$-wave shows a behavior which may be useful for the development of nondestructive testing methods for partially saturated soils. In dependence on the saturation it slightly linearly decreases and approximately doubles its value for high degrees of saturation. The speeds do not differ for drying and wetting. For small saturation the $P1$-speed for sand is approximately 1400 m/s, for silt loam around 1200 m/s. The two curves for increasing values of the saturation are nearly parallel.

An influence of the hysteresis in the capillary pressure curve is visible for the speeds of $P2$- and $P3$-wave. These speeds behave oppositely. While the $P2$-wave has a minimum for a certain degree of saturation (for both soil types in the region of 95%), the $P3$-wave shows a maximum for the same degree of saturation. The existence of a minimum in the speed of sound in air-water-mixtures is well known for a long time (e.g. [12]) and occurs in a comparable way also in partially saturated porous media.

Generally, the speeds of the pore-fluid driven waves are much less than those of the solid driven waves. The $P2$-wave speed lies in the range between 0 and 60 m/s, this of the $P3$-wave between 0 and 0.5 m/s. The maximum values are higher for silt loam than for sand and also

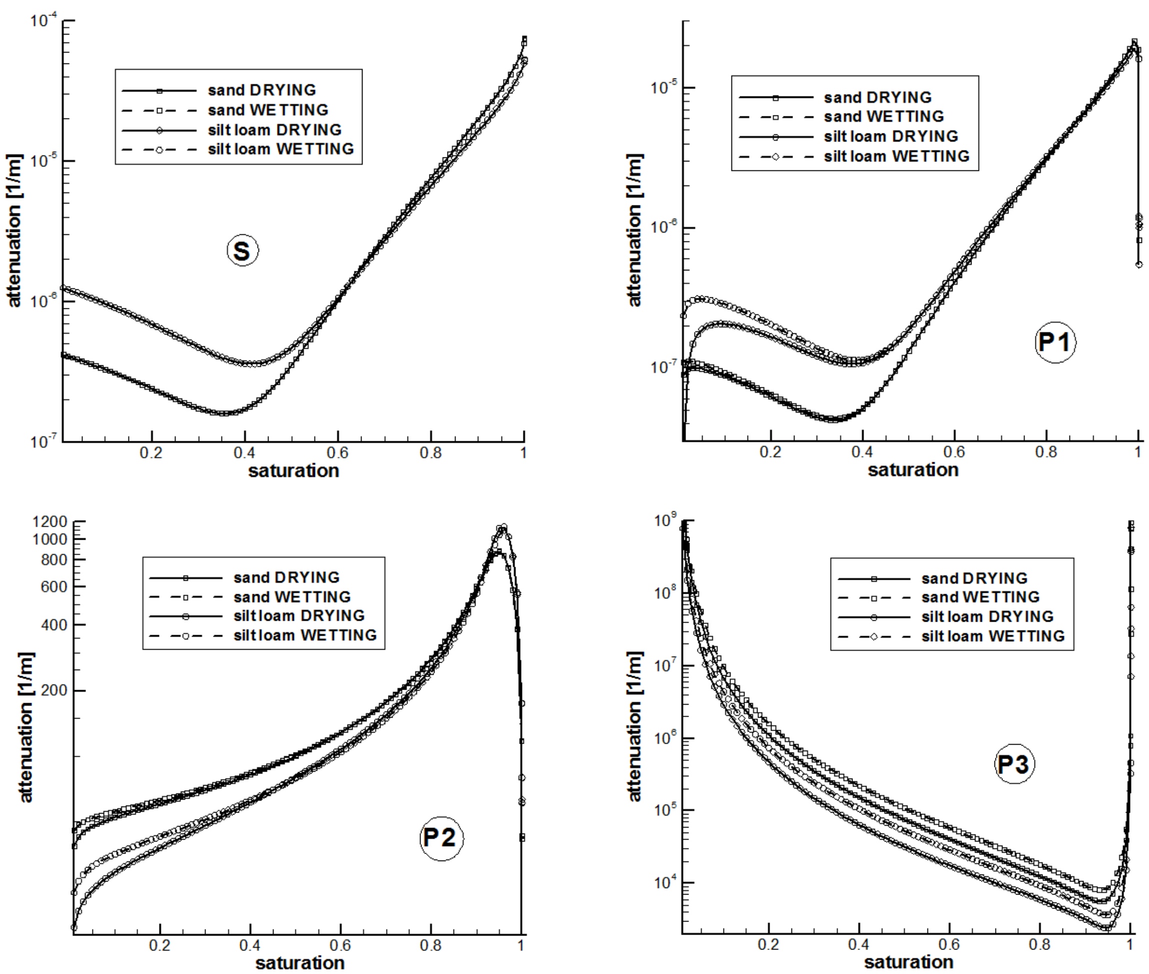

Figure 5. Attenuations of the transversal wave S and the three longitudinal waves $P1$, $P2$ and $P3$ in dependence on the initial saturation S_0 using the parameters of the MDC (solid lines) and MWC (dashed lines) for Del Monte sand (squares) and silt loam (circles); $\omega = 1000$ Hz.

the differences between drying and wetting are more pronounced for silt loam than for sand. Namely, the maximum value for the $P2$-speed for drying in silt loam is approximately 60 m/s, for wetting 42 m/s. Thus, the difference is around 30% whereas the values of 26 and 22 m/s in sand result in a difference of approximately 15%. Also for the speed of the $P3$-wave a difference nearly twice as big as for sand is observed for silt loam. While the differences occur for the $P2$-wave in the region of low saturations, for the $P3$-wave it happens in the region of high degrees of saturation.

The differences in the attenuations are not that obvious as for the speeds. Again, S- and $P1$-wave are little attenuated. Values between 10^{-7} and 10^{-4} 1/m appear. All curves exhibit a minimum at a degree of saturation of approximately 40%. For the shear wave drying and wetting curves do not show a difference, for low values of the saturation the attenuation of silt loam is higher than this for sand; for saturations higher than approximately 50% the attenuations of the two soil types are nearly the same. This behavior can be also observed for the attenuations of the $P1$-wave. Interestingly, for small degrees of saturation, for this wave in silt loam a difference between drying and wetting is visible (for the speed this was not the case). For the sand this behavior is barely observable.

As mentioned above, the $P2$-wave and, particularly, the $P3$-wave are strongly attenuated. The attenuations of these waves exhibit maxima for degrees of saturation at which the speed shows minima and vice versa. The attenuations of silt loam are slightly smaller than those of sand. While for the $P3$-wave the attenuation for drying and wetting differs for both soil types in nearly the whole range of saturations (except for the limit values), for the $P2$-wave this is only the case for small degrees of saturation.

Conclusions and outlook

In [10] the influence of the hysteresis in the capillary pressure curve already had been studied on the example of Del Monte sand filled by an air-water mixture. Four waves, one transversal wave and three longitudinal waves, had been analyzed. For the waves driven mainly by the skeleton (the shear wave and the fastest longitudinal wave) it could be shown that – as expected – the influence of the use of either drying or wetting data is negligible. However, for the pore fluid driven waves a smaller influence than expected had been emerged. Several possible reasons for this behavior had been mentioned: that the porosity had been chosen rather small, that only one soil type had been investigated and that the prediction of the main wetting curve had not been proven by experimental data.

By investigation of a second soil type and with a choice of material parameters which seems much more plausible, in this paper, a significant influence of drying and wetting on the propagation of sound waves in silt loam could be observed. It could be imagined that the influence in silt loam, indeed, is considerably larger than in sand. However, more likely, the reason of the small influence in sand is the choice of the material parameters.

In order to clarify the above mentioned questions, measurements of the main drying and wetting curves of the twelve soil types studied in [6] have been requested in a laboratory and will be interpreted theoretically once available. Then, several soil types for which significant material parameters are available can be compared, the quality of the prediction of the main curves can be checked and a sufficient number of soil types can be analyzed.

Acknowledgments

Financial support as an Einstein Junior Fellow by the Einstein Foundation Berlin is highly appreciated.

Journal of Physics: Conference Series **727** (2016) 012001 doi:10.1088/1742-6596/727/1/012001

References

[1] Albers B 2014 Modeling the hysteretic behavior of the capillary pressure in partially saturated porous media – a review, *Acta Mechanica* **225**(8), 2163–89

[2] Albers B 2015 Main drying and wetting curves of soils - on measurements, prediction and influence on wave propagation, accepted for publication in *Engineering Transactions*

[3] Haverkamp R, Reggiani P, Ross PJ and Parlange, J-Y 2002 Soil water hysteresis prediction model based on theory and geometric scaling. In *Environmental Mechanics, Water, Mass and Engergy Transfer in the Biosphere*, PAC Raats, D Smiles, AW Warrick, Ed. 213–46

[4] Van Genuchten MT 1980 A closed-form equation for predicting the hydraulic conductivity of unsaturated soils. *Soil Sci. Soc. Am. J.* **44**:892–8

[5] Lewis RW and Schrefler BA 1998 *The finite element method in the static and dynamic deformation and consolidation of porous media*. Wiley, Chichester

[6] Albers B 2010 *Modeling and Numerical Analysis of Wave Propagation in Saturated and Partially Saturated Porous Media*. Habilitation thesis, Shaker Verlag, Aachen

[7] Liakopoulos AC 1966 Theoretical approach to the solution of the infiltration problem. *International Association of Scientific Hydrology* **11**(1) 69–110

[8] Albers B 2010 Micro-Macro Transition and Linear Wave Propagation in Three-Component Compacted Granular Materials, AIP Conference Proceedings of the Joint IUTAM-ISIMM Symposium on Mathematical Modeling and Physical Instances of Granular Flows, vol. 1227, JD Goddard, JT Jenkins, P Giovine (Eds.), Melville, New York, 391-404

[9] White JE 1983 *Underground sound. Application of seismic waves, Methods in Geochemistry and Geophysics*. Vol. 18. Elsevier, Amsterdam, New York

[10] Albers B 2014 On modeling three-component porous media incorporating hysteresis, Proceedings of the 11th. World Congress on Computational Mechanics (WCCM XI), paper 2568

[11] Kelder O and Smeulders D 1996 Measurement of ultrasonic bulk properties of water-saturated porous media, in: EAGE, 58th Conference and Technical Exhibition, Amsterdam

[12] Wood, AB 1957 *A Textbook of Sound*. G. Bell and Sons, London